

Article

The Roles of Precursor-Induced Metal–Support Interaction on the Selective Hydrogenation of Crotonaldehyde over Ir/TiO₂ Catalysts

Aiping Jia ^{1,2,†}, Hantao Peng ^{1,†}, Yunshang Zhang ¹, Tongyang Song ³, Yanwen Ye ², Mengfei Luo ², Jiqing Lu ^{2,*} and Weixin Huang ^{1,4,*}

¹ Hefei National Laboratory for Physical Sciences at the Microscale, Key Laboratory of Surface and Interface Chemistry and Energy Catalysis of Anhui Higher Education Institutes, CAS Key Laboratory of Materials for Energy Conversion, Department of Chemical Physics, University of Science and Technology of China, Hefei 230026, China; aipingjia@zjnu.cn (A.J.); hantaop@mail.ustc.edu.cn (H.P.); zhys123@mail.ustc.edu.cn (Y.Z.)

² Key Laboratory of the Ministry of Education for Advanced Catalysis Materials, College of Chemistry and Life Sciences, Zhejiang Normal University, Jinhua 321004, China; yeyanwen1997@163.com (Y.Y.); mengfeiluo@zjnu.cn (M.L.)

³ Shanghai Key Laboratory of Green Chemistry and Chemical Processes, Chemistry and Molecular Engineering, East China Normal University, Shanghai 200062, China; 52184300049@stu.ecnu.edu.cn

⁴ Dalian National Laboratory for Clean Energy, Dalian 116023, China

* Correspondence: jiqinglu@zjnu.cn (J.L.); huangwx@ustc.edu.cn (W.H.); Tel.: +86-579-8228-7325 (J.L.); +86-551-6360-0435 (W.H.)

† These authors contributed equally.



Citation: Jia, A.; Peng, H.; Zhang, Y.; Song, T.; Ye, Y.; Luo, M.; Lu, J.; Huang, W. The Roles of Precursor-Induced Metal–Support Interaction on the Selective Hydrogenation of Crotonaldehyde over Ir/TiO₂ Catalysts. *Catalysts* **2021**, *11*, 1216. <https://doi.org/10.3390/catal11101216>

Academic Editor: Leonarda Francesca Liotta

Received: 25 August 2021
Accepted: 6 October 2021
Published: 9 October 2021

Publisher's Note: MDPI stays neutral with regard to jurisdictional claims in published maps and institutional affiliations.



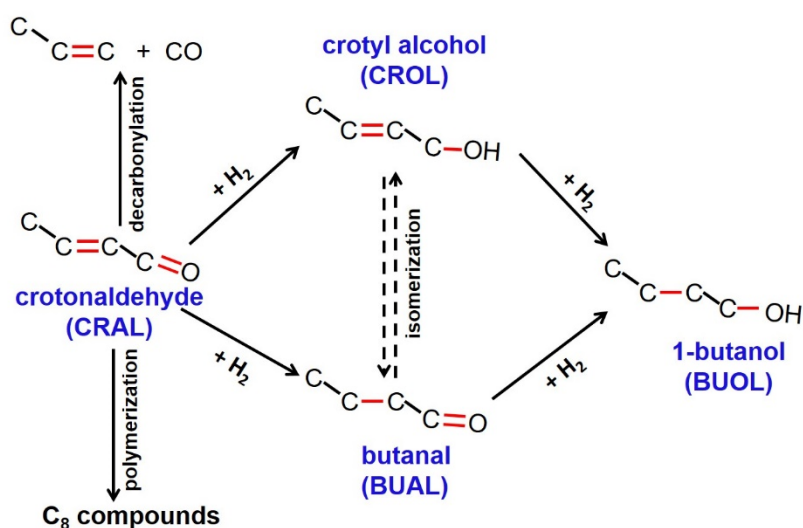
Copyright: © 2021 by the authors. Licensee MDPI, Basel, Switzerland. This article is an open access article distributed under the terms and conditions of the Creative Commons Attribution (CC BY) license (<https://creativecommons.org/licenses/by/4.0/>).

Abstract: Various supported Ir/TiO₂ catalysts were prepared using different Ir precursors (i.e., H₂IrCl₆, (NH₄)₂IrCl₆ and Ir(acac)₃) and tested for vapor phase selective hydrogenation of crotonaldehyde. The choice of Ir precursor significantly altered the Ir–TiO_x interaction in the catalyst, which thus had essential influences on the geometric and electronic properties of the Ir species, reducibility, and surface acidity, and, consequently, their reaction behaviors. The Ir/TiO₂-N catalyst using (NH₄)₂IrCl₆ as the precursor gave the highest initial reaction rates and turnover frequencies of crotyl alcohol formation. Such high performance was ascribed to the high Ir dispersion and high surface concentration of Ir⁰ species, as well as a higher surface acidity, in the Ir/TiO₂-N catalyst compared to its counterparts, indicating the synergistic roles of the Ir–TiO_x interface in the reaction, as the interfacial sites were responsible for the adsorption/activation of H₂ and the C=O bond in the crotonaldehyde molecule.

Keywords: crotonaldehyde; hydrogenation; Ir/TiO₂; iridium precursor; reaction mechanism

1. Introduction

The selective hydrogenation of α , β -unsaturated aldehyde to unsaturated alcohol is an important reaction in the industry of pharmaceuticals, and fragrances [1,2] as the α , β -unsaturated alcohols are useful chemicals and intermediates. Compared to the traditional synthesis employing strong reductants (e.g., LiAlH₄ and NaBH₄), using H₂ as reductants in the selective hydrogenation is eco-friendly and atom-economic. Crotonaldehyde (CRAL) is one of the representative α , β -unsaturated aldehyde. The possible reaction routes during the hydrogenation of CRAL are illustrated in Scheme 1. Nevertheless, the hydrogenation of the C=O bond to form the target product, i.e., crotyl alcohol (CROL), is much more difficult than the hydrogenation of the C=C bond to form butanal (BUAL) due to both thermodynamic and kinetic facts [3]. Hence, it is significant yet challenging to develop highly effective catalysts in the selective hydrogenation of CRAL.



Scheme 1. The hydrogenation reaction routes of crotonaldehyde (CRAL).

Noble metals (e.g., Pt [4–9], Au [10], Ru [11] and Ir [12–14]) supported on reducible oxides (e.g., TiO_2 [4–6,12–14], Ga_2O_3 [7], CeO_2 [8,10] and ZnO [9,11]) are efficient catalysts in the hydrogenation of CRAL. The behaviors of these catalysts can be modulated by metal–support interactions (MSI), which are used to accelerate the hydrogenation of the $\text{C}=\text{O}$ bond by creating the metal–support interfacial sites [4,12,14]. The nature of such a metal–support interface could be tuned in various ways, and one of the approaches is the choice of the metal precursors. It is well known that the nature of the metal precursor significantly affects the properties of the catalyst and its catalytic performance in the hydrogenation of CRAL, although their roles are sometimes debatable. For example, according to Gebauer-Henke et al. [7], Pt/ Ga_2O_3 catalysts prepared from chlorine-free $\text{Pt}(\text{acac})_2$ precursor showed much higher activity and selectivity to CROL than those prepared from H_2PtCl_6 , probably due to the formation of smaller Pt particle size in the former. The same group [8] also reported that the Pt/ CeO_2 catalyst prepared using $\text{Pt}(\text{NH}_3)_4(\text{NO}_3)_2$ as the precursor gave much higher selectivity but lower activity than those prepared using H_2PtCl_6 and $\text{Pt}(\text{NH}_3)_4(\text{Cl})_2 \cdot \text{H}_2\text{O}$ as the precursors, probably due to the formation of CePt_5 species in the former catalyst, which was favorable for the hydrogenation of $\text{C}=\text{O}$. Moreover, the choice of proper precursors is related to the nature of the support. For example, Wang et al. [9] reported that the Pt/ ZnO catalyst prepared from H_2PtCl_6 showed much higher activity and selectivity than those prepared from chlorine-free $\text{Pt}(\text{NH}_3)_4(\text{NO}_3)_2$ and residual chlorine played an important role in promoting the catalysts towards high selectivity to CROL.

The above-mentioned works reflect the fact that the choice of the metal precursor is crucial for the hydrogenation of CRAL, and thus, this investigation is worthwhile. It should be noted that even though the properties of catalysts can be modified by different metal precursors, the role of metal precursor on the catalytic behaviors could be significantly interfered with by the complexity of the surface of reducible oxides (with multiple crystal planes exposed) [15,16]. Fortunately, recent advances in the synthesis of oxide nanocrystals with uniform and well-defined morphologies have brought up new opportunities for more unambiguous investigation. For example, anatase TiO_2 nanocrystals with 98% {101}-crystal-plane exposed could be synthesized successfully [14], and this oxide has shown promising potential in the selective hydrogenation of CRAL. In our recent work [14], we prepared various Ir catalysts supported on anatase TiO_2 exposing different crystal planes (e.g., {101}, {100} and {001} planes) and compared their reaction behaviors in the hydrogenation of CRAL. It was found that the higher concentration of oxygen deficiency in the Ir/ TiO_2 -{101} could effectively improve the catalytic performance compared to the Ir/ TiO_2 -{001}. Moreover, the choice of Ir as the active noble metal for the selective hydrogenation of

CRAL is because Ir catalysts are more selective compared to Pt and Au catalysts in the CRAL hydrogenation [12,17–20] and other α , β -unsaturated aldehyde [21]. Moreover, the performance of the Ir-based catalysts could be improved by the addition of promoters. For example, Tamura et al. [22] reported that the addition of various promoters such as ReO_x , MoO_x , FeO_x and NbO_x significantly enhanced the activity of the Ir/ SiO_2 catalyst. On a NbO_x -promoted Ir/ SiO_2 catalyst (with an Ir/Nb molar ratio of 2/1), the CRAL conversion (41.6%) was six-fold higher than that of the bare Ir/ SiO_2 (7.3%), and the turnover frequency (TOF) on the NbO_x -promoted Ir catalyst was as high as 0.21 s^{-1} at $80 \text{ }^\circ\text{C}$. Similar findings were also reported in our previous works [18,23,24].

Although Ir/ TiO_2 catalysts are appealing in the hydrogenation of CRAL [14] as well as different carbonyl compounds [12,13,25,26], unfortunately, there are few reports on the effects of Ir precursors on the reaction behaviors of the Ir catalysts in selective hydrogenation. Therefore, in the current work, we prepared three different Ir/ TiO_2 catalysts using different Ir precursors, i.e., chlorine-containing $\text{Ir}(\text{NH}_4)_2\text{Cl}_6$ and H_2IrCl_6 and chlorine-free $\text{Ir}(\text{acac})_3$. Additionally, anatase TiO_2 nanocrystals dominantly exposing the {101} plane were used as the support. These catalysts were tested for CRAL hydrogenation to illustrate the roles of Ir precursors. It was found that the interaction between the Ir precursor and TiO_2 support during the preparation process exerted great influence on the properties of the catalysts, which consequently changed the catalytic behaviors.

2. Experimental

2.1. Synthesis of Anatase TiO_2 Nanocrystals and Preparation of Ir/ TiO_2 Catalysts

Anatase TiO_2 nanocrystals (NCs) dominantly exposing {101} plane were synthesized following the procedures reported by Liu et al. [27] and Chen et al. [28] Firstly, TiCl_4 solution (6.6 mL) was added dropwise to an aqueous solution of HCl (0.43 mol l^{-1} , 20 mL) at $0 \text{ }^\circ\text{C}$. After being stirred for 0.5 h, the solution was added dropwise into an aqueous solution of $\text{NH}_3 \cdot \text{H}_2\text{O}$ (5.5 wt.%, 50 mL) under continuous stirring at room temperature. Then the pH value of the solution was adjusted to 6–7 by an appropriate amount of aqueous $\text{NH}_3 \cdot \text{H}_2\text{O}$ (4 wt.%), after which the system was stirred for another 2h at room temperature. The resulting precipitate was filtered, washed repeatedly with deionized water until no residual Cl^- could be detected and dried at $70 \text{ }^\circ\text{C}$ for 12 h to acquire $\text{Ti}(\text{OH})_4$ precursor. Then $\text{Ti}(\text{OH})_4$ (2.0 g) and NH_4Cl (0.2 g) were dispersed together in a mixture of H_2O (15 mL) and *i*-PrOH (15 mL) under stirring at room temperature, and the mixture was transferred into a 50 mL Teflon-lined stainless steel autoclave and kept at $180 \text{ }^\circ\text{C}$ for 24 h. The resulting white precipitate was collected, washed repeatedly by deionized water and finally dried at $70 \text{ }^\circ\text{C}$ overnight to obtain the TiO_2 oxide without further calcination.

The supported Ir/ TiO_2 catalysts were prepared by an incipient wetness impregnation method using three different Ir precursors, i.e., iridium(III) acetylacetonate ($\text{Ir}(\text{acac})_3$), chloroiridic acid (H_2IrCl_6), ammonium hexachloroiridate ($(\text{NH}_4)_2\text{IrCl}_6$). Typically, 1.0 g TiO_2 -{101} NCs were added into a certain amount of Ir precursors solution (H_2IrCl_6 and $(\text{NH}_4)_2\text{IrCl}_6$ were dissolved in deionized water, and $\text{Ir}(\text{acac})_3$ was dissolved in benzene) under continuously stirring for 3 h, followed by aging statically for 3 h at ambient temperature. After the solvent in the mixture was evaporated using a water bath ($90 \text{ }^\circ\text{C}$), followed by drying overnight at $110 \text{ }^\circ\text{C}$. The solid was further calcined in static air at $400 \text{ }^\circ\text{C}$ for 4 h (at a ramp of $5 \text{ }^\circ\text{C min}^{-1}$) to obtain the catalysts. Since the decomposition temperature of $\text{Ir}(\text{acac})_3$ is around $300 \text{ }^\circ\text{C}$ based on the TG/DSC results, as shown in Figure S1, and also to avoid the sublimation of $\text{Ir}(\text{acac})_3$ during the calcination process, the catalyst employing $\text{Ir}(\text{acac})_3$ as precursor should first be calcined at $300 \text{ }^\circ\text{C}$ for 4 h with a low heating rate ($0.5 \text{ }^\circ\text{C min}^{-1}$) and then $400 \text{ }^\circ\text{C}$ for another 4h. The nominal Ir contents in the catalysts were about 5 wt.%, and the resulting catalysts were denoted as Ir/ TiO_2 -A, Ir/ TiO_2 -Cl and Ir/ TiO_2 -N, for $\text{Ir}(\text{acac})_3$, H_2IrCl_6 and $(\text{NH}_4)_2\text{IrCl}_6$ as the precursors, respectively.

2.2. Catalyst Characterizations

The actual Ir contents in the catalysts were measured by an inductively coupled plasma atomic emission spectrometer (ICP-AES, Optima 7300DV). The specific surface areas of the catalysts were measured by N₂ adsorption at 77 K on a Quantachrome Nova 4000e surface area analyzer. X-ray powder diffraction (XRD) was performed on a Bruker D8 ADVANCE powder X-ray with Cu K α radiation (40 kV, 40 mA), with a scan rate of 0.02° s⁻¹ and a 2 θ range of 10–90°. Before the measurements, the samples were subjected to pre-reduction in a H₂ flow (99.999%, 18 mL min⁻¹) at 300 °C for 1 h. The High-resolution transmission electron microscopy (HRTEM) was conducted on a JEM-2100F microscopy using an operation voltage of 200 kV. Prior to the HRTEM measurements, the samples were subjected to pre-reduction in the H₂ atmosphere (99.999%, 18 mL min⁻¹) at 300 °C for 1 h. The distribution of Ir particle size was determined based on counting no less than 200 Ir particles in each catalyst. The formula of $d_{VA} = \sum_i n_i d_i^3 / \sum_i n_i d_i^2$ (d_i , the experimentally determined particle size; n_i , the number of Ir particles with d_i) was used to calculate the volume-area mean diameter of Ir particles.

Hydrogen temperature-programmed reduction (H₂-TPR) experiment was carried out on an automatic chemisorption analyzer of MicrotracBEL Belcat II. The catalyst (50 mg) was loaded in a quartz tubular reactor and heated up to 300 °C and kept at 300 °C in a flow of pure O₂ (30 mL min⁻¹) for 0.5 h, followed by purging with pure Ar flow (99.99%, 30 mL min⁻¹) for another 0.5 h to clean the catalyst surface. After the sample was cooled down to room temperature, it was heated to 700 °C at a heating rate of 10 °C min⁻¹ in a 5% H₂-95% Ar mixture (30 mL min⁻¹). The H₂ consumption of each sample was calculated based on the H₂ consumption of 5.0 mg CuO powder.

Ammonia temperature-programmed desorption (NH₃-TPD) was performed on a Micromeritics AutoChem II chemisorption analyzer to determine the surface acidity of the catalyst. Before the measurement, the catalyst (200 mg) was pre-reduced in high purity of H₂ flow (99.999%, 18 mL min⁻¹) at 300 °C for 1 h. Then it was cooled down to 60 °C in a high purity N₂ flow (99.99%, 30 mL min⁻¹), followed by introducing a flow of NH₃ (30 mL min⁻¹) into the reactor for 0.5 h. Then the sample was heated from 60 to 100 °C and kept at 100 °C in the high purity N₂ flow (30 mL min⁻¹) for 0.5 h to remove the residual gaseous or physical adsorbed NH₃ on the catalyst surface. Then the sample was heated to 700 °C in a pure N₂ flow (30 mL min⁻¹) at a ramp of 10 °C min⁻¹. The surface acidic amounts of each sample were also calculated with a given NH₃ volume based on their peak areas of NH₃-desorption.

In situ X-ray photoelectron spectra (in situ-XPS) of the catalysts were recorded on an ESCALAB 250Xi spectrometer using a monochromatic Al anode K α radiation as X-ray source (1486.6 eV). C1s core level at 284.8 eV was used as the reference to calibrate the obtained binding energies. Before the measurements, the sample was firstly reduced in a pretreatment chamber with a flow of pure H₂ (99.999%, 18 mL min⁻¹) at 300 °C for 1 h and then cooled down to room temperature. Then the pre-reduced sample was transferred to the analysis chamber for measurement without being exposed to air.

Electron Paramagnetic Resonance (EPR) spectra of the catalysts were recorded on a JEOL JESFA 200 EPR spectrometer at 130 K using 1 mW of microwave power and 249.5 to 399.5 mT of sweep width. The modulation amplitude and frequency were 0.35 mT and 100 kHz, respectively. The samples were pre-reduced at 300 °C for 1 h using a flow of H₂ (99.999%, 18 mL min⁻¹) in a home-made fixed-bed reactor with a quartz tubular microreactor, and the whole microreactor was placed in the Ar-filled glovebox (Mikrouna Co. Ltd., China, O₂ concentrations below 0.1 ppm). After treatment and cooling to room temperature, the inlet and outlet of the processing gas were closed to prevent exposure to air. Afterwards, a 30 mg powder sample was taken out from the quartz tubular and sealed into an electron spin resonance (ESR) sample tube in the Ar-filled glovebox.

In situ CO chemisorption diffuse reflectance infrared Fourier transform spectra (in situ CO-DRIFTS) measurements of the samples were performed on a Nicolet iS50 FTIR spectrometer equipped with a PIKE DRIFT accessory. Before the measurement, the sample

was pre-reduced in a H₂ flow (99.999%, 18 mL min⁻¹) at 300 °C for 1 h, followed by heating in a N₂ flow (99.99%, 30 mL min⁻¹) for another 1 h. After that, the sample was cooled down to 30 °C and then exposed to the flow of 1%CO–99% N₂ mixture (20 mL min⁻¹) for 10 min. Then the sample was purged by a N₂ flow (99.99%, 30 mL min⁻¹) for 1 h to remove gaseous or physical adsorbed CO and then the spectra were recorded at 30 °C.

In situ Fourier transform infrared spectroscopy (in situ FTIR) of CRAL hydrogenation was also carried out on the same Nicolet iS50 FTIR spectrometer. Prior to the experiment, approximately 20 mg of the sample was pressed into a self-supported wafer (i.d. = 13 mm) and then loaded in a quartz IR cell. Thereafter, the sample was pre-reduced in a H₂ flow (99.999%, 18 mL min⁻¹) at 300 °C for 1 h, followed by heating in a N₂ flow (99.99%, 30 mL min⁻¹) for another 1 h. After the sample was cooled down to 30 °C in the flow of N₂, the CRAL vapor in the saturate CRAL vapor generator was introduced to the sample with a flow of H₂ (99.999%, 26 mL min⁻¹) for 10 min, followed by purging with the N₂ flow for 1 h to remove the residual CRAL in the IR cell. Then the H₂ flow (99.999%, 26 mL min⁻¹) was introduced, and the spectra were collected as a function of time kept at 30 °C.

2.3. Catalytic Reaction

The selective hydrogenation of gas-phase CRAL at atmospheric pressure was carried out using a fixed-bed quartz tube reactor (i.d. = 8 mm). Five milligrams of the catalyst diluted with one hundred ninety-five silica was loaded into the reactor with a thermal couple placed in the middle of the catalyst bed. Prior to each test, the sample was pre-reduced in the flow of H₂ (99.999%, 18 mL min⁻¹) at 300 °C for 1 h. After the reactor was cooled to the reaction temperature (80 °C), CRAL vapor was continuously introduced into the reactor by a flow of H₂ (99.999%, 26 mL min⁻¹). Since the saturate CRAL vapor generator was maintained at 0 °C, in the feed stream, the concentration of CRAL was 1 mol%, and the total pressure was 0.1MPa with a space velocity of 7800 mL g_{cat}⁻¹h⁻¹. The gas line was heated above 50 °C to avoid any CRAL condensation. The CRAL and reaction products were measured online by a Shimadzu GC-2014 gas chromatography equipped with an FID detector.

3. Results and Discussion

3.1. Characterizations of the Catalyst

Table 1 lists the physical properties of the catalysts. The catalysts have similar surface areas of ca. 90 m² g⁻¹. The actual Ir contents of these catalysts are close to 5 wt%.

Table 1. The summary of physical properties of TiO₂-{101} NCs and various pre-reduced Ir/TiO₂ catalysts.

Catalysts	S _{BET} /m ² g ⁻¹	Ir Content ^a /wt.% ^a	d _{VA} /nm	D _{Ir} ^b / %	Surface Cl/Ti Molar Ratio ^c	
					Calcined	Pre-Reduced
Ir/TiO ₂ -A	92	4.93	1.7	64.7	n.d.	n.d.
Ir/TiO ₂ -Cl	89	4.90	1.5	73.3	0.056	0.005
Ir/TiO ₂ -N	90	4.86	1.3	84.6	0.061	0.006
TiO ₂	98	-	-	-	-	-

^a: The actual Ir contents in catalysts were determined by ICP-AES; ^b: Calculated based on the formula of D_{Ir} (Ir dispersion) = 1.1/d_{VA};

^c: Calculated based on Cl_{2p} and Ti_{2p} peaks derived from XPS results. The calcined catalysts determined by XPS without any pre-treatment were denoted as Calcined and after pre-reduction were denoted as Pre-reduced.

Both the fresh TiO₂ oxide and pre-reduced Ir/TiO₂ catalysts show similar XRD patterns, which were ascribed to anatase TiO₂ (JCPDS No. 21-1272) [29], as shown in Figure 1. Moreover, the diffractions of Ir or IrO_x species cannot be detected in these catalysts, suggesting high Ir dispersions in the catalysts.

Figure 2 shows the HRTEM images of fresh TiO₂ NCs and pre-reduced Ir/TiO₂ catalysts with their Ir particle size distributions. The as-synthesized TiO₂ NCs (Figure 2a1–a2) have sizes between 15–30 nm, and the lattice fringes resolved in the HRTEM images all arise from those of anatase TiO₂, which is consistent with the XRD results. The percentage of {101} facet in the TiO₂ was estimated to be around 98% based on the previously proposed

procedure [14] (Supporting Information, Figure S1), suggesting that the TiO_2 -{101} NCs could be employed as ideal support with homogeneous surface features. As shown in Figure 2b–d, the loading of Ir and further thermal treatment barely have an effect on the morphologies of the TiO_2 NCs. It is certain that the Ir particles are highly dispersed on the surface of Ir/ TiO_2 catalysts with mean diameters (d_{VA}) of ca. 1.3–1.7 nm. However, the particle size of the Ir NPs in the catalysts varies slightly. As shown in Figure 2b2–d2 and Table 1, the Ir/ TiO_2 -N catalyst exhibits the highest Ir dispersion of 84.6% and the smallest mean particle size of 1.3 nm compared to those of Ir/ TiO_2 -A and Ir/ TiO_2 -Cl. Thus, it is clear that the Ir precursors impose an effect on the geometrical structure of the Ir species, and the smallest Ir particle size in the Ir/ TiO_2 -N could safely lead to a conclusion that the MSI in the Ir/ TiO_2 -N might be stronger than those in the other two catalysts.

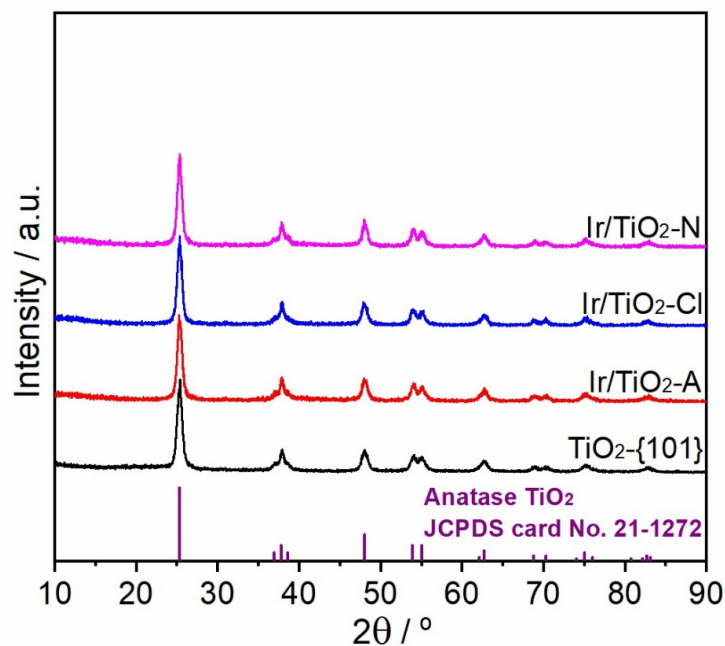


Figure 1. XRD patterns of fresh TiO_2 -{101} NCs and pre-reduced Ir/ TiO_2 catalysts.

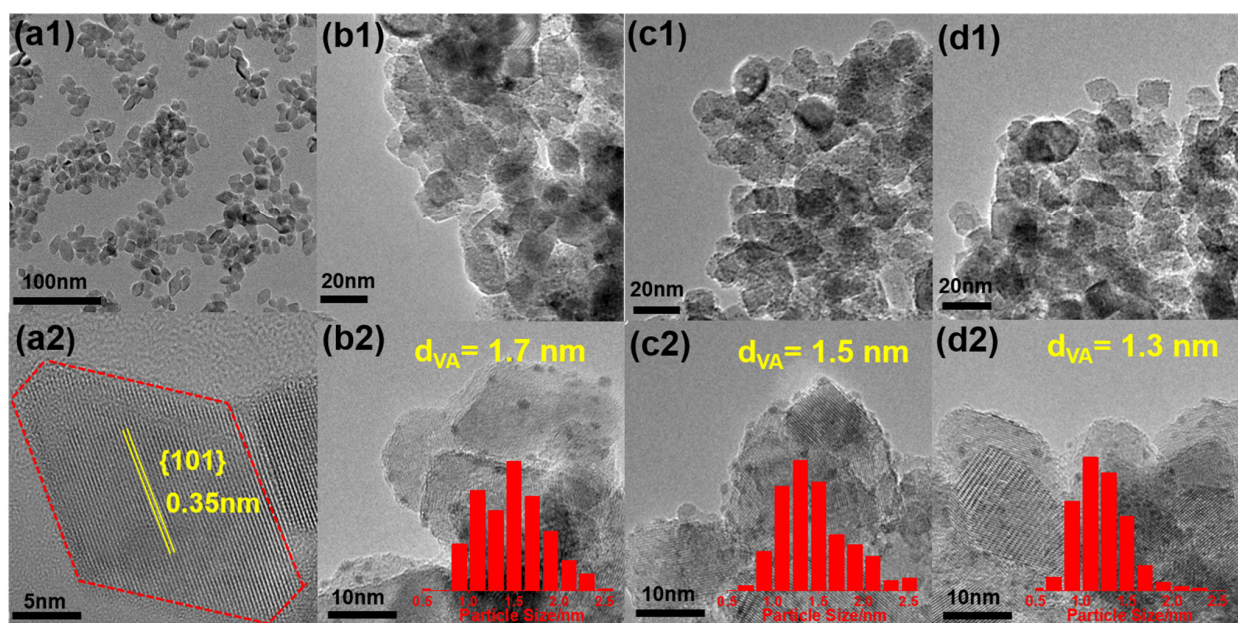


Figure 2. HRTEM images and Ir particle size distributions of (a1,a2) fresh TiO_2 -{101}, pre-reduced (b1,b2) Ir/ TiO_2 -A, (c1,c2) Ir/ TiO_2 -Cl and (d1,d2) Ir/ TiO_2 -N catalysts.

The H₂-TPR profiles for the fresh TiO₂ NCs and the Ir/TiO₂ catalysts are shown in Figure 3a. The bare TiO₂ NCs could hardly be reduced, so we expect that a weak reduction at ca. 650 °C is observed due to the reduction in surface TiO₂. However, three reduction peaks at 143 °C (α), 256 °C (β) and 328 °C (γ) are observed for the Ir/TiO₂-A catalyst, while the α peak could not be observed in the Ir/TiO₂-Cl and Ir/TiO₂-N catalysts. For the Ir/TiO₂-A catalyst, the α peak could be assigned to the reduction of IrO_x into a less strong IrO_x-TiO_x interaction, as it contains large IrO_x species (Figure 2b1–b2). The β and γ peaks could be ascribed to the reduction of IrO_x and/or IrCl_x species in a stronger IrO_x(IrCl_x)-TiO₂ interaction [13,14] due to these Ir species are more difficult to be reduced. For the Ir/TiO₂-Cl and Ir/TiO₂-N catalysts, the absence of the α peak indicates that the Ir species in these catalysts are in stronger IrO_x(IrCl_x)-TiO₂ interaction compared to those in the Ir/TiO₂-A catalyst. Moreover, the β and γ peaks on the Ir/TiO₂-N catalyst generally shift to lower temperatures compared to those on the Ir/TiO₂-Cl and Ir/TiO₂-A catalyst, and such easier reduction is probably due to its higher Ir dispersion (Figure 2d1–d2). The H₂ consumptions (1.12–1.28 mmol g⁻¹) of the catalysts are evidently higher than the nominal value (0.50 mmol g⁻¹, assuming that all the Ir species are IrO₂ in the fresh catalyst), thus demonstrating the reduction of TiO₂ is supported by the typical spillover effect. Furthermore, the reducibility of these different Ir/TiO₂ catalysts could rank as follows: Ir/TiO₂-N (1.28 mmol g⁻¹) > Ir/TiO₂-Cl (1.26 mmol g⁻¹) > Ir/TiO₂-A (1.12 mmol g⁻¹), implying the prominent effect of metal precursors on the reducibility of catalysts. This behavior could be correlated with a higher Ir dispersion, as shown in Figure 2, and thus a stronger Ir-TiO_x interaction in these catalysts, which promotes their redox properties, particularly the co-reduction of TiO₂ oxide.

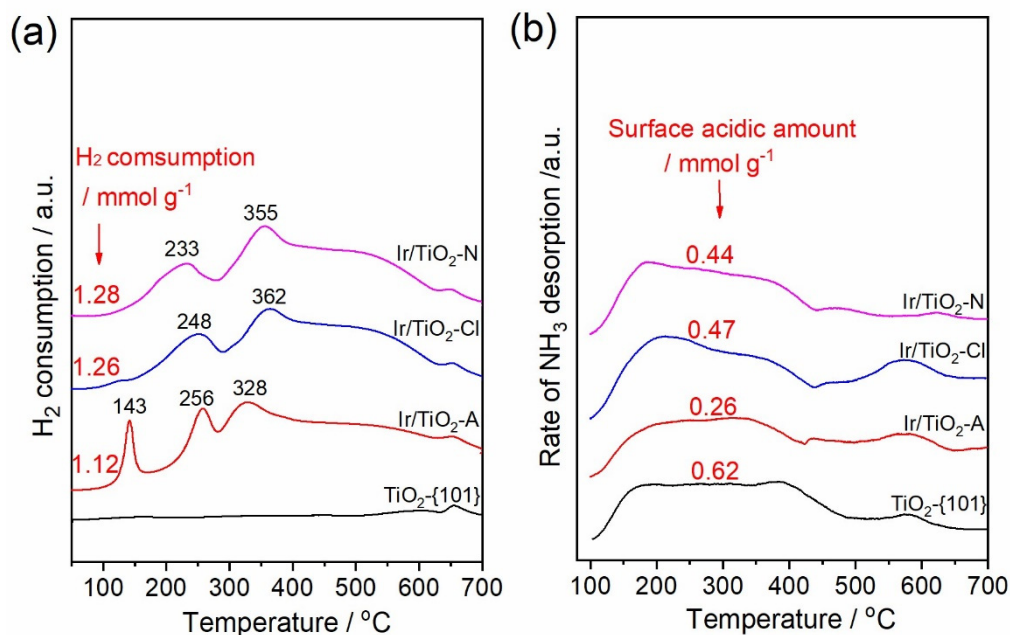


Figure 3. (a) H₂-TPR and (b) NH₃-TPD profiles of pre-reduced bare TiO₂-{101} NCs and Ir/TiO₂ catalysts.

The pre-reduced TiO₂ support exhibits NH₃ desorption peaks between 100–600 °C in the NH₃-TPD profile as shown in Figure 3b, demonstrating that there are different strength acid sites on the catalysts surface, i.e., weak acid sites in 100–200 °C, medium acid sites in 200–400 °C and strong acid sites in 400–600 °C. The loading of Ir on the support barely changes the feature of the NH₃ desorption pattern, but the quantity of the surface acid sites decreases obviously in comparison to that of the TiO₂ support, probably due to the surface coverage by Ir species. Based on the quantitative results shown in Figure 3b, the Ir/TiO₂-A gives the lowest surface acidity (0.26 mmol g⁻¹), which is almost half of that

of Ir/TiO₂-Cl (0.47 mmol g⁻¹), while the Ir/TiO₂-N gives slightly lower surface acidity (0.44 mmol g⁻¹). It should also be noted that there are many factors that could affect the acidity of the catalyst, such as surface oxygen vacancy, residual chlorine species, and the oxidized Ir species (Ir^{δ+}). Among these factors, the surface oxygen vacancy could be a key factor, as demonstrated in our previous work [14]. The Ir/TiO₂-N catalyst with higher Ir dispersion but higher acidity compared to that of the Ir/TiO₂-A could be due to its much higher redox ability, as shown in the H₂-TPR results (Figure 3a), in which easier co-reduction of TiO₂ oxide produces a higher concentration of surface oxygen vacancy.

The surface Ir⁰ and Ir^{δ+} species contents were determined based on Ir 4f core level XPS spectra of pre-reduced Ir/TiO₂ catalysts, as shown in Figure 4. It should be noted that the Ir 4f spectra are overlapped by obvious Ti 3s peaks. In spite of this, the Ir 4f_{7/2} spectrum can be deconvoluted to two peaks ascribed to Ir⁰ and Ir^{δ+} species, respectively, at BEs of 60.6–60.9 eV and 61.9–62.1 eV [12]. The surface Ir⁰/Ir^{δ+} ratio in the Ir/TiO₂-N (26.0) is significantly higher than those in the Ir/TiO₂-Cl (7.1) and Ir/TiO₂-A (4.4). This observation is consistent with the H₂-TPR results (Figure 3a), as the Ir/TiO₂-N possesses the highest H₂ consumption (although the H₂ consumption includes the co-reduction of TiO₂ adjacent to the Ir species), which further suggests the influence of precursors on the electronic properties of the Ir species. Additionally, the surface analyses reveal that the fresh Ir/TiO₂-Cl and Ir/TiO₂-N catalysts contain a certain content of residual chlorine species with surface Cl/Ti ratios of 0.056–0.061, as shown in Table 1, which was ascribed to the incomplete decomposition of the H₂IrCl₆ precursor during the static calcination. However, the much smaller surface Cl/Ti ratios (ca. 0.005, Table 1) in the pre-reduced catalysts means the pre-reduction by H₂ could remove the majority of the residual chlorine species. Therefore, it could be considered that the effect of residual chlorine on the catalytic behavior was negligible.

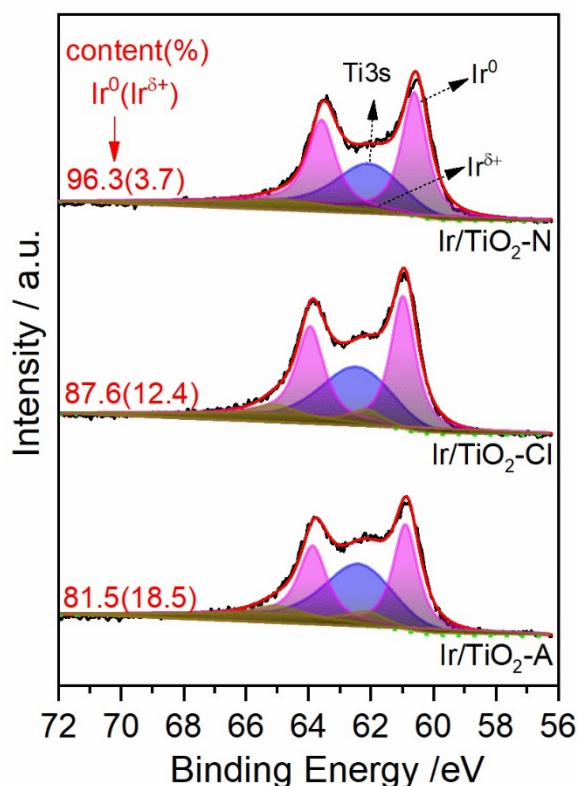


Figure 4. Ir 4f core level XPS spectra of pre-reduced Ir/TiO₂ catalysts.

The in situ CO-DRIFTS technique was employed to further probe the electronic properties of the Ir species in the pre-reduced Ir/TiO₂ catalysts. As shown in Figure 5a, the catalysts give similar bands of CO adsorption. In detail, bands at ca. 2072–2077 cm⁻¹ and

2015–2042 cm^{-1} are ascribed to CO linearly adsorbed on highly coordinated Ir^0 located on single-crystal planes and low coordinated Ir^0 located on the edges and corners [30–32], respectively. Additionally, the band at 2072 cm^{-1} in the Ir/TiO₂-A blue shifts to 2077 cm^{-1} in the Ir/TiO₂-N, indicating that the stronger interaction of Ir NPs with the support in the latter, which is consistent with the H₂-TPR results.

The defect structures of the pre-reduced bare TiO₂ NCs and Ir/TiO₂ catalysts were determined by the EPR technique. As shown in Figure 5b, all the Ir/TiO₂ catalysts as well as the TiO₂ support exhibit a distinct feature at $g = 2.002$ ascribed to the oxygen vacancy with one electron (F^{1+} color center) [33]. As shown in Figure 5b, the intensities of F^{1+} color center in the pre-reduced Ir/TiO₂ catalysts are all slightly weaker than that of bare TiO₂ probably due to the surface oxygen vacancy covered by the Ir NPs, which decreases the signal of the F^{1+} color center in the former. In addition, some new weak signals due to the surface Ti^{3+} signal (g_{\perp} -type feature, $\text{Ti}_{\text{surf}}^{3+}$) at $g = 1.968$ appear all over these Ir/TiO₂ catalysts, indicating that Ti^{4+} can be reduced to Ti^{3+} on the catalyst surface in the presence of Ir due to the typical spillover effect [34,35]. Nevertheless, the intensities of F^{1+} in the Ir/TiO₂-Cl and Ir/TiO₂-N catalysts are slightly stronger than that in the Ir/TiO₂-A, indicating the relatively higher oxygen vacancy concentration in the former since it is widely believed that the concentrations of the F^{1+} color center represent the relative concentration of oxygen vacancy [36], which is probably due to their relatively better redox ability, as demonstrated by H₂-TPR results (Figure 3a).

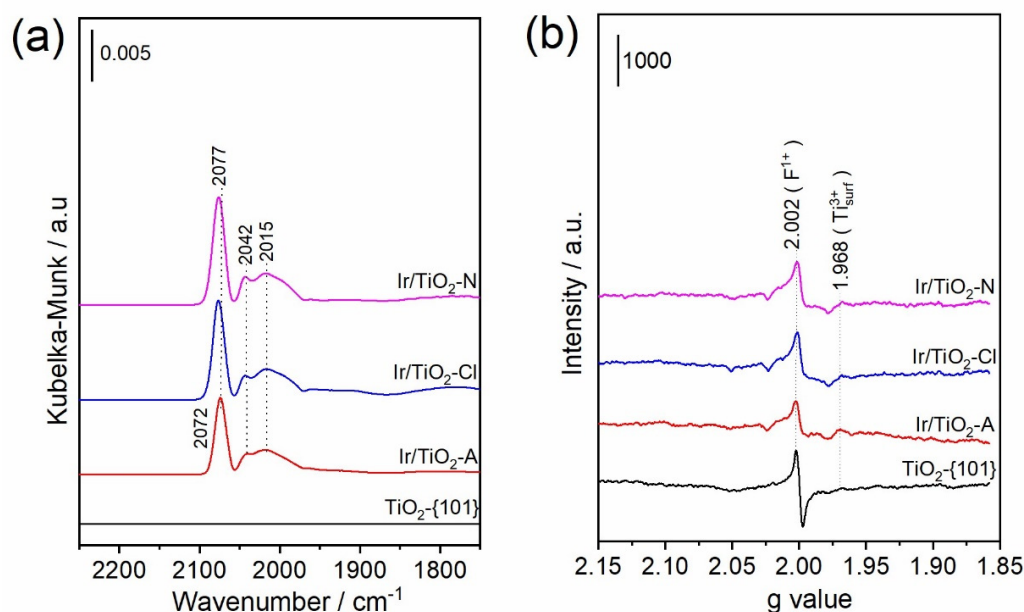


Figure 5. (a) in situ DRIFTS of CO adsorption at 30 °C and (b) EPR spectra at 130 K of the pre-reduced bare TiO₂-{101} NCs and Ir/TiO₂ catalysts. (Note: the EPR intensity comparisons of different samples were carried out based on the same loading (ca. 30 ± 1 mg)).

3.2. Catalytic Behaviors of the Catalysts

Figure 6 illustrates the reaction behaviors of the catalysts. The bare TiO₂ NCs are inactive at a reaction temperature of 80 °C. For Ir/TiO₂ catalysts, regardless of the employed precursor, both activity and selectivity were evidently improved, especially in the initial stage (after 30 min reaction). The main products are a target product CROL (with a selectivity of ca. 60–75%), and the by-products are BUAL (with a selectivity of ca. 20–30%), BUOL (with a selectivity of ca. 3–5%), C3 (i.e., propylene and propane) and C8 (2,4,6-octatrienal) compounds (with a selectivity of ca. 2–3%). All the catalysts suffer deactivation during the reaction process due to the formation of coke deposits from the starting products parallel to the main hydrogenation reaction[12], but the reaction reaches a quasi-steady state after 180 min. Comparison of the behaviors of the different Ir/TiO₂ catalysts (Figure 6a–c)

reveals that the initial CRAL conversion ranks as follows: Ir/TiO₂-N (14.8%) > Ir/TiO₂-Cl (12.1%) > Ir/TiO₂-A (5.1%), while the selectivity to CROL remains relatively constant (60–70%). Similar trends are also observed during the quasi-steady state. Figure 6d–e also compares the reaction rates and turnover frequencies (TOFs) of the catalysts at different stages. At the initial stage (TOS = 30 min, Figure 6d), the Ir/TiO₂-N gives the highest rate of 108.2 $\mu\text{mol}_{\text{CRAL}} \text{g}_{\text{Ir}}^{-1} \text{s}^{-1}$ and the highest TOF_{Ir} of 0.0174 s⁻¹ (for CROL formation), while the Ir/TiO₂-A catalyst gives the lowest rate of 36.9 $\mu\text{mol}_{\text{CRAL}} \text{g}_{\text{Ir}}^{-1} \text{s}^{-1}$ and the lowest TOF of 0.0078 s⁻¹. Therefore, the Ir/TiO₂-N shows a three-fold higher reaction rate and two-fold TOF than Ir/TiO₂-A, suggesting the crucial roles of the Ir precursors on the reaction. Moreover, Ir/TiO₂-N gives the best performance in the extended reaction period, as shown in Figure 6e–f.

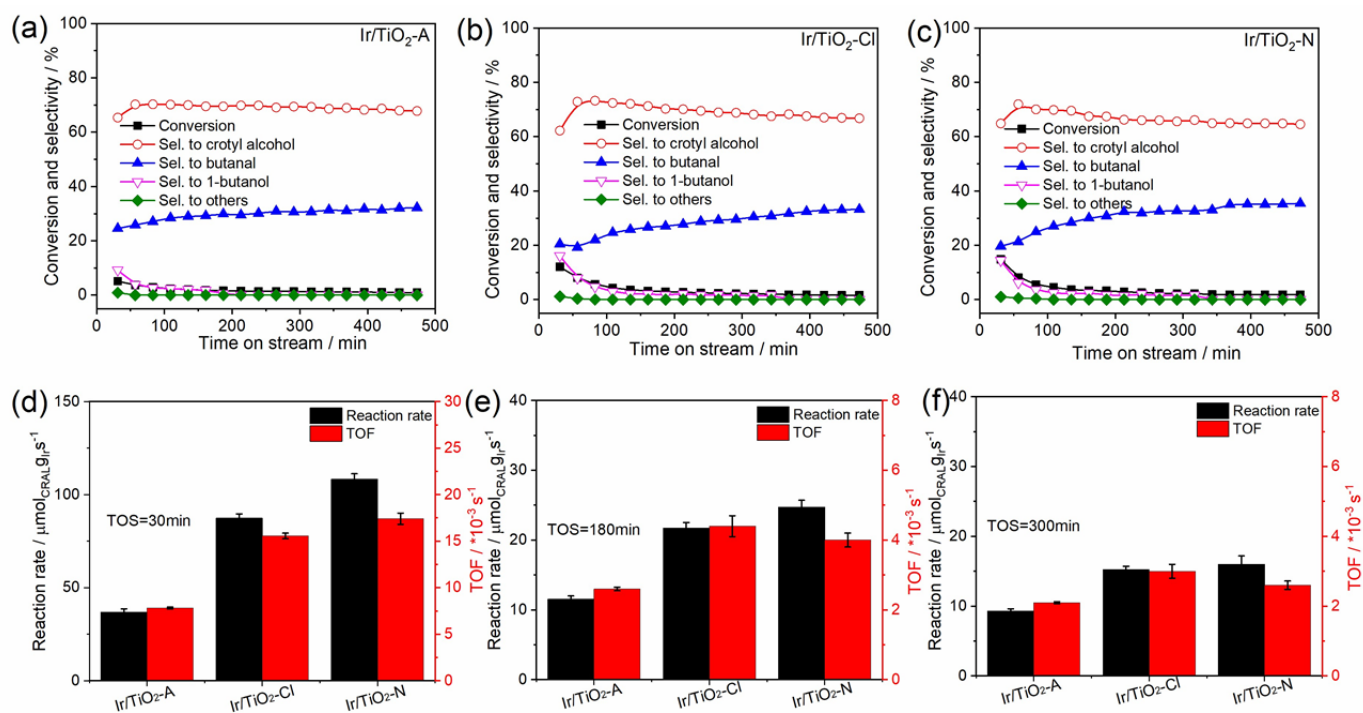


Figure 6. (a–c) Time course of selective hydrogenation of vapor phase CRAL over the pre-reduced Ir/TiO₂ catalysts and (d–f) comparison of their CRAL reaction rates and CROL formation TOF at time on stream (TOS) of 30, 180 and 300 min. (Reaction condition: catalyst loading: 5 mg diluted with 195 mg silica, reaction temperature = 80 °C; total flow rate = 26 mL min⁻¹; CRAL content = 1 mol.%).

The performance of the different Ir/TiO₂ catalysts and other reported Ir-based catalysts applied in the gas-phase hydrogenation of crotonaldehyde were summarized in Table 2. As shown in Table 2, the majority of these catalysts were subjected to pre-reduction by H₂ atmosphere at 300 °C as the best performance could be obtained using this reduction temperature [13,14]. Meanwhile, the reaction rate of the Ir/TiO₂-N catalyst is comparable to the result reported by Yuan et al. [18], giving a value of 24.7 $\mu\text{mol} \text{g}_{\text{Ir}}^{-1} \text{s}^{-1}$. Concerning the turnover frequency for the CROL formation, the values obtained on the Ir/TiO₂ catalysts in the current works ($2.6\text{--}4.4 \times 10^{-3} \text{s}^{-1}$) are comparable to those on bare supports (e.g., $3.8 \times 10^{-3} \text{s}^{-1}$ on the Ir/TiO₂ [13]). However, they are lower than those obtained on the promoted Ir catalysts (e.g., $16.9 \times 10^{-3} \text{s}^{-1}$ on the 3Ir-0.05(Cr-Fe)/SiO₂ [18] and $18.0 \times 10^{-3} \text{s}^{-1}$ on the 3Ir-0.1Fe/SiO₂ [23]), which could be ascribed to the much higher Ir dispersions in the current work (64.7–84.6%, Table 1) than those in 3Ir-0.05(Cr-Fe)/SiO₂ (29.0%) [18] and 3Ir-0.1Fe/SiO₂ (23.5%) [23].

Table 2. Summary of reaction results over various Ir-based catalysts.

Sample ^a	Reduction Temperature/°C	Reaction Time/min	Reaction Rate ^b /μmol g _{Ir} ⁻¹ s ⁻¹	TOF ^c /×10 ⁻³	Selectivity /%			Reference
					Crotyl Alcohol	Butanal	Others ^d	
Ir/TiO ₂ -A	300	180	11.5	2.6	70.1	29.9	0	This work
Ir/TiO ₂ -Cl	300	180	21.7	4.4	71.3	27.0	1.7	This work
Ir/TiO ₂ -N	300	180	24.7	4.1	69.5	28.8	1.7	This work
Ir/TiO ₂	300	500	16.2	3.8	74.6	14.6	10.8	[13]
Ir/ZrO ₂	500	180	8.7	7.6	82.2	8.1	9.7	[37]
3Ir0.1Fe/SiO ₂	300	600	23.8	18.0	90.8	3.7	5.5	[23]
3Ir-0.05(Cr-Fe)/SiO ₂	300	600	27.1	16.9	85.9	8.3	5.8	[18]
3Ir-0.05Fe/BN	300	180	16.4	6.7	84.4	9.0	6.6	[24]
Ir-NbO _x /SiO ₂ (Nb/Ir = 0.5)	500	120	48.4	210	92.8	3.7	3.0	[22]

^a All these catalysts were applied in the gas-phase hydrogenation of crotonaldehyde. Except for Ir-NbO_x/SiO₂ (Nb/Ir = 0.5) catalyst, the reaction temperature is 100 °C, and the others are 80 °C; ^b moles of crotonaldehyde converted per gram of Ir per second; ^c TOF = moles of crotyl alcohol formed per mole of exposed metal sites based on Ir dispersion per second; ^d Others are butanol, C8 compounds (2,4,6-octatrienal) and C3 compounds (propane and propylene).

3.3. In Situ FTIR Studies of CRAL Reaction over Ir/TiO₂ Catalysts

An in situ FTIR spectroscopic study was conducted in order to investigate the effect of Ir precursor on the CRAL reaction properties of the Ir/TiO₂ catalysts. As shown in Figure 7, the FTIR bands of CRAL hydrogenation over the Ir/TiO₂ catalysts are mainly located in three regions, i.e., 1950–2060, 1500–1800 and 1350–1450 cm⁻¹. The weak bands in the 1950–2060 cm⁻¹ region could be assigned to irreversibly adsorbed CO on various metallic Ir species due to the decarbonylation of CRAL. The bands in the 1500–1800 cm⁻¹ region are the features of stretching vibrations of C=C and C=O bonds in the CRAL molecule. In detail, two weak bands located at 1710 and 1725 cm⁻¹ could be ascribed to the $\nu(\text{C}=\text{O})$ bond of the residual gaseous CRAL molecule [17,19] in the IR cell, which could not be completely removed by the flow of N₂. The bands at 1656–1658 and 1675–1682 cm⁻¹ are assigned to CRAL adsorbed via the C=O bond in di- σ_{CO} mode [12] and π_{CO} mode [4], respectively. The band at ca. 1642 cm⁻¹ could be ascribed to the di- σ_{CC} mode of CRAL adsorption via C=C bond [4]. These results demonstrated that CRAL molecules can adsorb on Ir/TiO₂ surface via both C=O and C=C bonds. In addition, we found that the intensities of the bands at 1658 and 1682 cm⁻¹ on the Ir/TiO₂-A catalyst are much lower than those on the Ir/TiO₂-Cl and Ir/TiO₂-N catalysts, suggesting that the C=O bond adsorption on the Ir/TiO₂-A catalyst is inhibited, probably due to its low acidity, as shown in Figure 3b. Moreover, bands at 1642, 1656–1658 and 1675–1682 cm⁻¹ for the Ir/TiO₂-Cl and Ir/TiO₂-N catalysts decline rapidly in intensities within 5 min, indicating a facile reaction between CRAL molecules and H₂. In addition, since the band at 1675–1682 cm⁻¹ still remains after 5 min while that at 1656–1658 cm⁻¹ completely disappears, it suggests that the hydrogenation of the C=O bond in the di- σ_{CO} adsorption configuration is easier than that in the π_{CO} adsorption configuration. The bands in the 1377–1450 cm⁻¹ region are ascribed to the symmetric and asymmetric $\delta(\text{C}-\text{H})$ vibration of methyl (CH₃-) groups [4,19], which are more prominent on the Ir/TiO₂-Cl and Ir/TiO₂-N compared to those on the Ir/TiO₂-A catalyst. However, for the Ir/TiO₂-A catalyst, the bands at 1682 and 1642 cm⁻¹ are so weak compared to those at 1377–1450 cm⁻¹ and rapidly disappear in 1 min, indicating that the hydrogenation reaction over the Ir/TiO₂-A catalyst is inhibited. Meanwhile, the bands in the region of 1900–2050 cm⁻¹ remain constant during the reaction, demonstrating strong CO adsorption on the surface Ir species, particularly in the Ir/TiO₂-Cl and Ir/TiO₂-N catalysts. Therefore, the strong CO adsorption may account for another reason for the catalyst deactivation during the reaction.

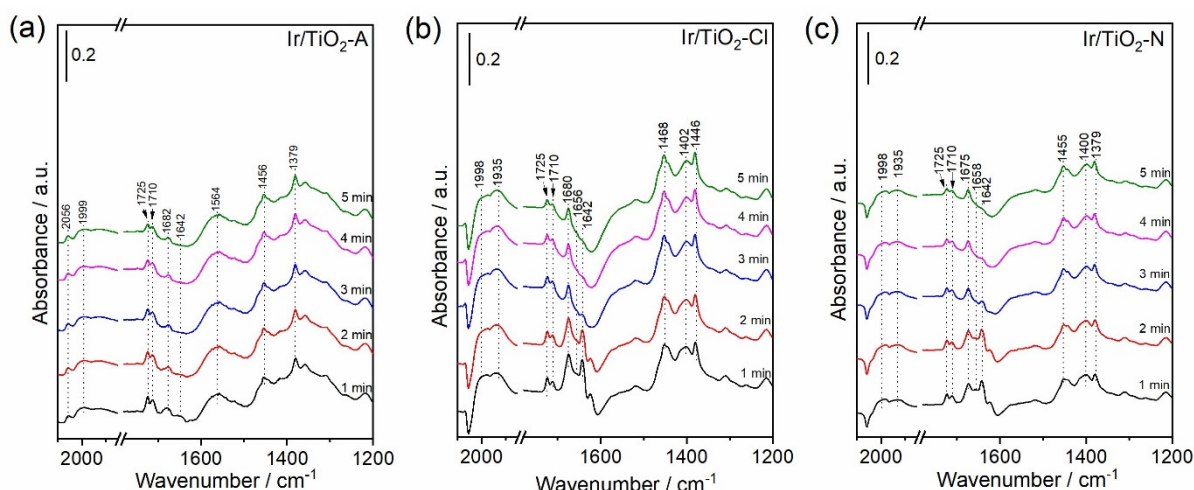


Figure 7. In situ FTIR spectra of CRAL hydrogenation reaction at 30 °C over the pre-reduced Ir/TiO₂ catalysts in region of 1200–2100 cm⁻¹.

3.4. Discussion on the Effect of Ir Precursors and Reaction Mechanisms

In the current work, we found that the Ir precursors exert a profound influence on the properties of the Ir/TiO₂ catalysts and, consequently, their reaction behaviors. The main conclusion could be drawn that the Ir/TiO₂ catalysts employing H₂IrCl₆ and (NH₄)₂IrCl₆ as the precursors give much better performance (both CRAL reaction rates and TOF for CROL formation) than the one using Ir(acac)₃ as the precursor. The Ir precursor significantly altered the Ir-TiO_x interactions, including Ir morphologies (Figure 2), reducibility (Figure 3a), surface acidity (Figure 3b), as well as electronic properties (Figures 4 and 5a). For CRAL hydrogenation over Ir supported on reducible oxides, such as TiO₂, the reaction takes place on the Ir-TiO_x interface, with the metallic Ir species offering sites for H₂ dissociation, while the partially reduced TiO_x with oxygen vacancies (working as Lewis acid sites) offering sites for CRAL adsorption. H₂ molecules are believed to dissociate heterolytically on metallic Ir species [22]. Therefore, a high concentration of metallic Ir species in the catalyst seems helpful in the H₂ dissociation. In the current work, the Ir⁰ concentrations in the Ir/TiO₂ catalysts (Figure 4) follow the order of Ir/TiO₂-N (96.3%) > Ir/TiO₂-Cl (87.6%) > Ir/TiO₂-A (81.5%), in parallel with their CRAL reaction rates and TOF of CROL formation, as shown in Figure 6d. These results also demonstrated that an increase in the amount of metallic Ir favors the catalytic activity. Moreover, it is well known that the adsorption features of CRAL on the catalyst surface play essential roles in determining both activity (adsorption strength) and selectivity (adsorption configuration), which is commonly related to the surface acidity of the catalyst [38]. Since the three catalysts give similar selectivity to CROL, it could be deduced that the CRAL adsorption geometries on these catalysts are similar. Indeed, the FTIR results (Figure 7) indicated that the main adsorption configuration of CRAL on the catalysts is via the C=O bond, which accounts for the observed high selectivity (ca. 70%) to CROL. Such C=O bond adsorption geometry is due to the interaction between the charge-enriched oxygen atom in the C=O bond and the Lewis acid sites on the catalyst surface, which has been well recognized and plays an essential role in the adsorption of the C=O bond in the CRAL molecule [12,14]. The high surface acidity of the Ir/TiO₂-N and Ir/TiO₂-Cl is responsible for their high activity, while the low surface acidity of the Ir/TiO₂-A leads to low activity. Therefore, the results clearly demonstrate the synergistic roles of the Ir-TiO_x interface in the reaction, which have been proposed previously by others [12].

4. Conclusions

This work demonstrates the strong effect of Ir precursors on the reaction behaviors of Ir/TiO₂ catalysts for CRAL hydrogenation. The Ir/TiO₂-N and Ir/TiO₂-Cl catalysts prepared using Cl-containing Ir precursors ((NH₄)₂IrCl₆ and H₂IrCl₆, respectively) are more active than that prepared using a Cl-free Ir(acac)₃ precursor, with the Ir/TiO₂-N using (NH₄)₂IrCl₆ precursor possessing the best performance. Such high activities are not related to the presence of residual chlorine species as their contents are very low. Instead, the improved activities are related to different Ir-TiO_x interactions induced by the Ir precursor. For example, the strong Ir-TiO_x interaction in the Ir/TiO₂-N catalyst results in the facile reduction of the IrO_x species as well as the adjacent TiO₂. Consequently, the presence of a high concentration of metallic Ir species is helpful in the dissociation of H₂, while the partially reduced Ti³⁺ and related oxygen vacancies generate surface acid sites for CRAL adsorption. Therefore, such an Ir-TiO_x interface plays a synergistic role in the reaction.

Supplementary Materials: The following are available online at <https://www.mdpi.com/article/10.3390/catal11101216/s1>, Figure S1: TG/DSC profiles for Ir(acac)₃.

Author Contributions: Conceptualization, J.L. and W.H.; methodology, H.P., Y.Z., T.S. and Y.Y.; software, A.J. and H.P.; validation, M.L., J.L. and W.H.; formal analysis, A.J.; investigation, A.J. and H.P.; resources, A.J. and H.P.; data curation, A.J. and H.P.; writing—original draft preparation, A.J.; writing—review and editing, J.L.; visualization, A.J.; supervision, J.L. and W.H.; project administration, J.L. and W.H.; funding acquisition, J.L. and W.H.. All authors have read and agreed to the published version of the manuscript.

Funding: This research was funded by the National Natural Science Foundation of China (No. 21525313, 21773212, 91945301 and 91745202) and the Chinese Academy of Sciences, the Changjiang Scholars Program of Ministry of Education of China.

Data Availability Statement: The study did not report any data, so no data availability was stated.

Conflicts of Interest: There are no conflicts to declare.

References

1. Claus, P. Selective Hydrogenation of α , β -Unsaturated Aldehydes and Other C=O and C=C Bonds Containing Compounds. *Top. Catal.* **1998**, *5*, 51–62. [[CrossRef](#)]
2. Lan, X.; Wang, T. Highly Selective Catalysts for the Hydrogenation of Unsaturated Aldehydes: A Review. *ACS Catal.* **2020**, *10*, 2764–2790. [[CrossRef](#)]
3. Mäki-Arvela, P.; Hájek, J.; Salmi, T.; Murzin, D.Y. Chemoselective Hydrogenation of Carbonyl Compounds over Heterogeneous Catalysts. *Appl. Catal. A* **2005**, *292*, 1–49. [[CrossRef](#)]
4. Dandekar, A.; Vannice, M.A. Crotonaldehyde Hydrogenation on Pt/TiO₂ and Ni/TiO₂ SMSI Catalysts. *J. Catal.* **1999**, *183*, 344–354. [[CrossRef](#)]
5. Delbecq, F.; Li, Y.; Loffreda, D. Metal–support Interaction Effects on Chemo–regioselectivity: Hydrogenation of Crotonaldehyde on Pt₁₃/CeO₂(1 1 1). *J. Catal.* **2016**, *334*, 68–78. [[CrossRef](#)]
6. Yang, X.; Mueannern, Y.; Baker, Q.A.; Baker, L.R. Crotonaldehyde Hydrogenation on Platinum–Titanium Oxide and Platinum–Cerium Oxide catalysts: Selective C=O Bond Hydrogen Requires Platinum Sites Beyond the Oxide–Metal Interface. *Catal. Sci. Technol.* **2016**, *6*, 6824–6835. [[CrossRef](#)]
7. Gebauer-Henke, E.; Grams, J.; Szubiabiewicz, E.; Farbotko, J.; Touroude, R.; Rynkowske, J. Pt/Ga₂O₃ Catalysts of Selective Hydrogenation of Crotonaldehyde. *J. Catal.* **2007**, *250*, 195–208. [[CrossRef](#)]
8. Abid, M.; Touroude, R. Pt/CeO₂ Catalysts in Selective Hydrogenation of Crotonaldehyde: High Performance of Chlorine-free Catalysts. *Catal. Lett.* **2000**, *69*, 139–144. [[CrossRef](#)]
9. Wang, D.; Ammari, F.; Touroude, R.; Su, D.S.; Schlögl, R. Promotion Effect in Pt–ZnO Catalysts for Selective Hydrogenation of Crotonaldehyde to Crotyl alcohol: A Structural Investigation. *Catal. Today* **2009**, *147*, 224–230. [[CrossRef](#)]
10. Campo, B.; Petit, C.; Volpe, M.A. Hydrogenation of crotonaldehyde on different Au/CeO₂ catalysts. *J. Catal.* **2008**, *254*, 71–78. [[CrossRef](#)]
11. Ramos-Fernández, E.V.; Silvestre-Albero, J.; Sepúlveda-Escribano, A.; Rodríguez-Reinoso, F. Effect of the Metal Precursor on the Properties of Ru/ZnO Catalysts. *Appl. Catal. A Gen.* **2010**, *374*, 221–227. [[CrossRef](#)]
12. Reyes, P.; Aguirre, M.C.; Melián-Cabrera, I.; Granados, M.L.; Fierro, J.L.G. Interfacial Properties of an Ir/TiO₂ System and Their Relevance in Crotonaldehyde Hydrogenation. *J. Catal.* **2002**, *208*, 229–237. [[CrossRef](#)]
13. Chen, P.; Lu, J.-Q.; Xie, G.-Q.; Hu, G.-S.; Zhu, L.; Luo, L.-F.; Huang, W.-X.; Luo, M.-F. Effect of Reduction Temperature on Selective Hydrogenation of Crotonaldehyde over Ir/TiO₂ Catalysts. *Appl. Catal. A Gen.* **2012**, *433–434*, 236–242. [[CrossRef](#)]
14. Jia, A.P.; Zhang, Y.S.; Song, T.Y.; Zhang, Z.H.; Tang, C.; Hu, Y.M.; Zheng, W.B.; Luo, M.F.; Lu, J.Q.; Huang, W.X. Crystal-plane Effects of Anatase TiO₂ on the Selective Hydrogenation of Crotonaldehyde over Ir/TiO₂ Catalysts. *J. Catal.* **2021**, *395*, 10–22. [[CrossRef](#)]
15. Gao, Y.X.; Wang, W.D.; Chang, S.J.; Huang, W.X. Morphology Effect of CeO₂ Support in the Preparation, Metal–Support Interaction, and Catalytic Performance of Pt/CeO₂ Catalysts. *ChemCatChem* **2013**, *5*, 3610–3620. [[CrossRef](#)]
16. Ying, Z.; Doronkin, D.E.; Chen, M.; Wei, S.; Grunwaldt, J.D. Interplay of Pt and Crystal Facets of TiO₂: CO Oxidation Activity and Operando XAS/DRIFTS Studies. *ACS Catal.* **2016**, *6*, 7799–7809. [[CrossRef](#)]
17. Tamura, M.; Tokonami, K.; Nakagawa, Y.; Tomishige, K. Selective Hydrogenation of Crotonaldehyde to Crotyl Alcohol over Metal Oxide Modified Ir Catalysts and Mechanistic Insight. *ACS Catal.* **2016**, *6*, 3600–3609. [[CrossRef](#)]
18. Yuan, J.F.; Luo, C.Q.; Yu, Q.; Jia, A.P.; Hu, G.S.; Lu, J.Q.; Luo, M.F. Great Improvement on the Selective Hydrogenation of Crotonaldehyde over CrO_x- and FeO_x-promoted Ir/SiO₂ catalysts. *Catal. Sci. Technol.* **2016**, *6*, 4294–4305. [[CrossRef](#)]
19. Xu, Y.M.; Zheng, W.B.; Hu, Y.M.; Tang, C.; Jia, A.P.; Lu, J.Q. The Effects of MoO_x Decoration on the Selective Hydrogenation of Crotonaldehyde over MoO_x-Promoted Ir/TUD-1 Catalysts. *J. Catal.* **2020**, *381*, 222–233. [[CrossRef](#)]
20. Tian, S.; Gong, W.; Chen, W.; Lin, N.; Zhu, Y.; Feng, Q.; Xu, Q.; Fu, Q.; Chen, C.; Luo, J.; et al. Regulating the Catalytic Performance of Single-Atomic-Site Ir Catalyst for Biomass Conversion by Metal–Support Interactions. *ACS Catal.* **2019**, *9*, 5223–5230. [[CrossRef](#)]

21. Lin, W.; Cheng, H.; Li, X.; Zhang, C.; Zhao, F.; Arai, M. Layered Double Hydroxide-like $Mg_3Al_{1-x}Fe_x$ Materials as Supports for Ir Catalysts: Promotional Effects of Fe Doping in Selective Hydrogenation of Cinnamaldehyde. *Chin. J. Catal.* **2018**, *39*, 988–996. [[CrossRef](#)]
22. Tamura, M.; Tokonami, K.; Nakagawa, Y.; Tomishige, K. Effective NbO_x -Modified Ir/SiO₂ Catalyst for Selective Gas-Phase Hydrogenation of Crotonaldehyde to Crotyl Alcohol. *ACS Sustain. Chem. Eng.* **2017**, *5*, 3685–3697. [[CrossRef](#)]
23. Yu, Q.; Bando, K.K.; Yuan, J.F.; Luo, C.Q.; Jia, A.P.; Hu, G.S.; Lu, J.Q.; Luo, M.F. Selective Hydrogenation of Crotonaldehyde over Ir-FeO_x/SiO₂ Catalysts: Enhancement of Reactivity and Stability by Ir-FeO_x Interaction. *J. Phys. Chem. C* **2016**, *120*, 8663–8673. [[CrossRef](#)]
24. Ning, X.; Xu, Y.M.; Wu, A.Q.; Tang, C.; Jia, A.P.; Luo, M.F.; Lu, J.Q. Kinetic Study of Selective Hydrogenation of Crotonaldehyde over Fe-promoted Ir/BN Catalysts. *Appl. Surf. Sci.* **2019**, *463*, 463–473. [[CrossRef](#)]
25. Reyes, P.; Rojas, H.; Fierro, J.L.G. Effect of Fe/Ir Ratio on the Surface and Catalytic Properties in Citral Hydrogenation on Fe-Ir/TiO₂ Catalysts. *J. Mol. Catal. A Chem.* **2003**, *203*, 203–211. [[CrossRef](#)]
26. Rojas, H.A.; Martínez, J.J.; Díaz, G.; Gómez-Cortés, A. The Effect of Metal Composition on the Performance of Ir-Au/TiO₂ Catalysts for Citral Hydrogenation. *Appl. Catal. A Gen.* **2015**, *503*, 196–202. [[CrossRef](#)]
27. Liu, L.; Gu, X.; Ji, Z.; Zou, W.; Tang, C.; Gao, F.; Dong, L. Anion-Assisted Synthesis of TiO₂ Nanocrystals with Tunable Crystal Forms and Crystal Facets and Their Photocatalytic Redox Activities in Organic Reactions. *J. Phys. Chem. C* **2013**, *117*, 18578–18587. [[CrossRef](#)]
28. Chen, S.; Abdel-Mageed, A.M.; Li, D.; Bansmann, J.; Cisneros, S.; Biskupek, J.; Huang, W.; Behm, R.J. Morphology-Engineered Highly Active and Stable Ru/TiO₂ Catalysts for Selective CO Methanation. *Angew. Chem. Int. Ed.* **2019**, *58*, 10732–10736. [[CrossRef](#)]
29. Liu, Y.; Wang, Z.; Wang, W.; Huang, W. Engineering Highly Active TiO₂ Photocatalysts via the Surface-Phase Junction Strategy Employing a Titanate Nanotube Precursor. *J. Catal.* **2014**, *310*, 16–23. [[CrossRef](#)]
30. Tanaka, K.; Watters, K.L.; Howe, R.F. Characterization of Supported Iridium Catalysts Prepared from Ir₄(CO)₁₂. *J. Catal.* **1982**, *75*, 23–38. [[CrossRef](#)]
31. López-De Jesús, Y.M.; Vicente, A.; Lafaye, G.; Marécot, P.; Williams, C.T. Synthesis and Characterization of Dendrimer-Derived Supported Iridium Catalysts. *J. Phys. Chem. C* **2008**, *112*, 13837–13845. [[CrossRef](#)]
32. Toolenar, F.J.C.M.; Bastein, A.G.T.M.; Ponc, V. The Effect of Particle Size in the Adsorption of Carbon Monoxide on Iridium: An Infrared Investigation. *J. Catal.* **1983**, *82*, 35–44. [[CrossRef](#)]
33. Okumura, M.; Coronado, J.M.; Soria, J.; Haruta, M.; Conesa, J.C. EPR Study of CO and O₂ Interaction with Supported Au Catalysts. *J. Catal.* **2001**, *203*, 168–174. [[CrossRef](#)]
34. Li, Y.; Xu, B.; Fan, Y.; Feng, N.; Qiu, A.; Miao, J.; He, J.; Yang, H.; Chen, Y. The Effect of Titania Polymorph on the Strong Metal-Support Interaction of Pd/TiO₂ Catalysts and Their Application in the Liquid Phase Selective Hydrogenation of Long Chain Alkadienes. *J. Mol. Catal. A Chem.* **2004**, *216*, 107–114. [[CrossRef](#)]
35. Conesa, J.C.; Soria, J. Reversible Ti³⁺ Formation by Hydrogen Adsorption on M/TiO₂ Catalysts. *J. Phys. Chem.* **1982**, *86*, 1392–1395. [[CrossRef](#)]
36. Huang, J.; He, S.; Goodsell, J.L.; Mulcahy, J.R.; Guo, W.; Angerhofer, A.; Wei, W.D. Manipulating Atomic Structures at the Au/TiO₂ Interface for O₂ Activation. *J. Am. Chem. Soc.* **2020**, *142*, 6456–6460. [[CrossRef](#)] [[PubMed](#)]
37. Zhu, L.; Hu, G.S.; Lu, J.Q.; Xie, G.Q.; Chen, P.; Luo, M.F. Effects of Ir Content on Selective Hydrogenation of Crotonaldehyde over Ir/ZrO₂ Catalysts. *Catal. Commun.* **2012**, *21*, 5–8. [[CrossRef](#)]
38. Ammari, F.; Lamotte, J.; Touroude, R. An Emergent Catalytic Material: Pt/ZnO Catalyst for Selective Hydrogenation of Crotonaldehyde. *J. Catal.* **2004**, *221*, 32–42. [[CrossRef](#)]